Journal of Cardiovascular Magnetic Resonance®, 4(2), 223–232 (2002)

METHODS

In Vivo Real-Time Intravascular MRI

Pedro A. Rivas,[1] Krishna S. Nayak,[2] Greig C. Scott,[2] Michael V. McConnell,[1] Adam B. Kerr,[2] Dwight G. Nishimura,[2] John M. Pauly,[2] and Bob S. Hu[1,*]

[1]*Division of Cardiovascular Medicine, Stanford University School of Medicine, 300 Pasteur Drive, Room H-2157, Stanford, CA 94305-5233*
[2]*Department of Electrical Engineering, Stanford University, Stanford, California*

ABSTRACT

Purpose. The Magnetic resonance imaging (MRI) is an emerging technology for catheter-based imaging and interventions. Real-time MRI is a promising method for overcoming catheter and physiologic motion for intravascular imaging.

Methods. All imaging was performed on a 1.5 T Signa MRI scanner with high-speed gradients. Multiple catheter coils were designed and constructed, including low-profile, stub-matched coils. Coil sensitivity patterns and SNR measurements were compared. Real-time imaging was performed with an interleaved spiral sequence using a dedicated workstation, providing real-time data acquisition, image reconstruction and interactive control and display. Real-time "black-blood" imaging was achieved through incorporation of off-slice saturation pulses. The imaging sequence was tested in a continuous flow phantom and then in vivo in the rabbit aorta using a 2 mm catheter coil.

Results. The real-time intravascular imaging sequence achieved 120–440 micron resolution at up to 16 frames per second. Low-profile stub-tuned catheter coils achieved similar SNR to larger traditional coil designs. In the phantom experiments, addition of real-time black-blood saturation pulses effectively suppressed the flow signal and allowed visualization of the phantom wall. In vivo experiments clearly showed real-time intravascular imaging of the rabbit aortic wall with minimal motion artifacts and effective blood signal suppression.

Conclusions. Real-time imaging with low-profile coil designs provides significant enhancements to intravascular MRI.

Key Words: *Magnetic resonance imaging; Intravascular; Atherosclerosis; Catheter coils*

*Corresponding author. Fax: (650) 725-7568; E-mail: hu@lad.stanford.edu

INTRODUCTION

While coronary angiography remains the clinical gold standard for evaluating patients for coronary artery disease, it does not directly image the disease itself, namely the atherosclerotic vessel wall. Luminal stenoses, as depicted by angiography, are predictive of chronic occlusion (1), but minor stenoses are often associated with acute myocardial infarction (2,3). Postmortem data suggest that plaque structure and composition, rather than stenosis severity, correlate with plaque vulnerability (4–6). Thus, directly imaging the coronary wall may be useful to predict risk and guide medical therapy and/or catheter-based interventions. It would also provide "pre-morbid" data to understand better plaque features associated with acute coronary events. Currently, intravascular ultrasound is the primary technique used to examine human coronary atherosclerosis in vivo (7), but its ability to provide detailed plaque characterization has been limited.

Magnetic resonance imaging (MRI) is a highly flexible imaging technology, which can provide detailed structural imaging with high soft tissue contrast. Accordingly, it has been shown to be superior to ultrasound in characterizing plaque (8,9). While progress has been made in noninvasive MRI of the coronary wall, spatial resolution has been limited to 0.5–0.8 mm (10–13). One approach to improving resolution is to match the receiver coil to the size of the region of interest, which achieves better SNR as the noise volume is reduced. Since Kantor first demonstrated the feasibility of catheter-based MRI (14), several research groups have developed intravascular MRI coils (15–20). A catheter coil, however, is subject to significant motion and blood flow artifacts, which has resulted in approaches that occlude blood flow and/or impinge on the vessel wall (21–24), which are clinically suboptimal in the coronary arteries. Real-time imaging is an alternative approach to avoid motion artifacts. Accordingly, we have developed real-time black-blood intravascular imaging in combination with low-profile, high-SNR coil geometries. This study demonstrates our results ex vivo and in vivo in the rabbit aorta.

METHODS

Magnetic Resonance Imaging Hardware

Imaging was performed on a 1.5 T Signa whole-body MRI scanner (General Electric Medical Systems, Milwaukee, WI) with advanced gradients (40 mT/m, 150 mT/m/msec). This system is augmented with a Sun workstation for real-time data acquisition, data transfer, image reconstruction, and interactive control, and display, as previously described (25). The quadrature body coil was used for RF transmission and the catheter coils were used for signal reception.

Catheter Coils

Initially, three coil prototypes similar to those previously reported were built and tested in our laboratory (Figs. 1 and 2). In the opposed solenoid design (Fig. 1a), two 7-mm long counter-wound loops were constructed from fine wire (34 awg) with a 6-mm gap between loops, resulting in overall length of 20 mm and a 4-mm diameter. The central gap between the two solenoids experiences a substantial radial protrusion of field lines with superior radial homogeneity at a cost of a fall-off in SNR outside of the central region (15,16). The twin-lead design (Fig. 1b) has the advantages of a smaller profile, longer FOV, and more flexibility for tortuous vessels (18). The imaging element is a two-conductor wire connected by a tuning capacitor at one end. The insulator between the wires forms the loop gap. Its larger longitudinal FOV allows for multislice axial imaging at the cost of reduced radial homogeneity. The tuning circuitry is also placed locally. The loopless coil (Fig. 1c) is a dipole antenna formed by unfolding a small coaxial outer and inner conductor (19). It can be placed into very small blood vessels with remote matching and tuning. These probes demonstrate other design aspects, specifically the use of thin coax (50 Ω characteristic impedance, 2.7-mm diameter), and remote location of Q spoiling and final matching circuitry with half-wavelength coax cable. The Q spoiling circuitry forces the coil into a high-impedance state when the PIN diode is switched on to prevent interaction with the high-power MRI transmitter.

In order to overcome the size limitation of fixed-coil capacitors, additional coil designs were developed based on solenoid (Fig. 1d) and twin-lead (Fig. 1e) imaging elements (26). These designs replace discrete capacitors with open-circuit transmission line stubs of 0.5-mm microcoaxial cable, whose lengths, which run parallel to the main coax, are then trimmed to tune the circuit. The smaller profile coax-stub-matched twin-lead catheter coil (Fig. 2) could fit into a standard 6 French (2 mm) introducer and was used for our flow phantom and in vivo rabbit experiments.

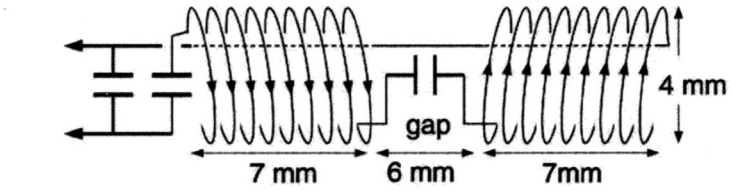

a) Opposed Solenoids

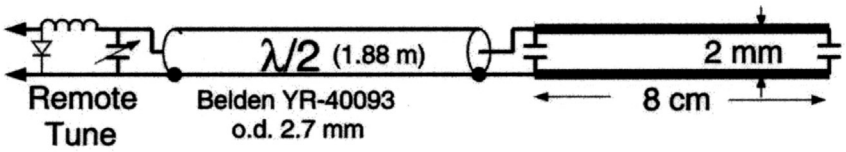

b) Twin Lead

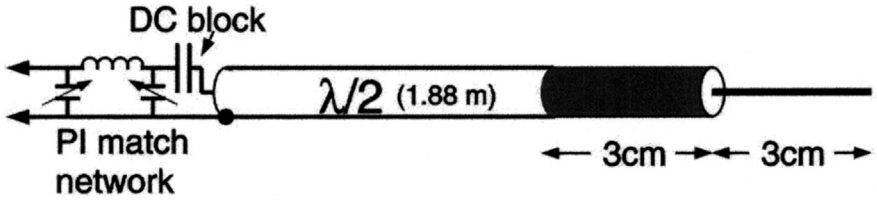

c) Loopless Probe

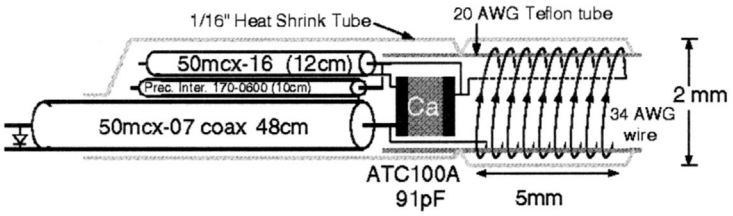

d) Coax-Stub-Matched Single Solenoid

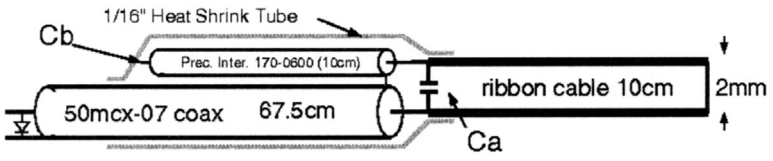

e) Coax-Stub-Matched Twin Lead

Figure 1. Schematics of the catheter coil designs.

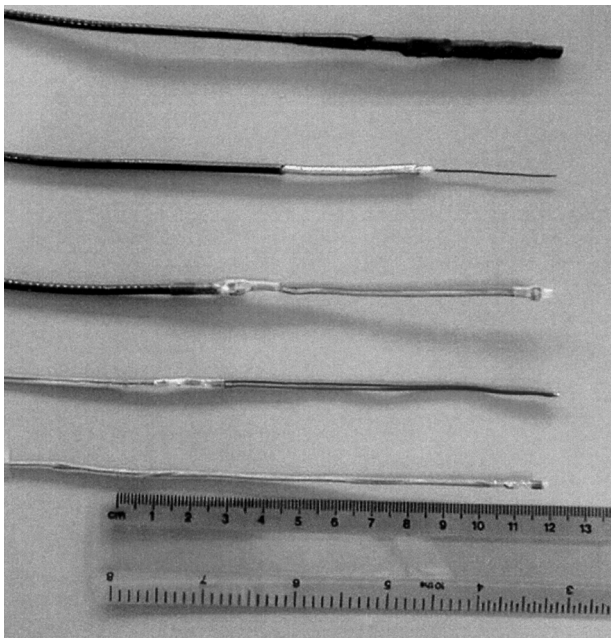

Figure 2. Catheter coils. From top to bottom: opposed solenoids, loopless probe, twin lead, coax-stub-matched twin lead, and coax-stub-matched single solenoid.

Image Acquisition

The real-time imaging system has been described previously (25). In general, a water-selective 7.68 msec spectral-spatial excitation is followed by spiral interleaved acquisitions. Spiral trajectories are used because of their efficient k-space coverage and good motion properties. The spiral interleaves can be adjusted for the desired readout duration and spatial/temporal resolution. Real-time images are reconstructed on a single multiprocessor machine. Each image consists of data from the previous 6–20 interleaves, as prescribed by the pulse sequence. The sliding window creates an image from the most recently acquired spirals at rates of up to 16 frames per second (27). Real-time control and display are implemented using an X-Window environment. Separate interactive sliders control FOV, flip angle, imaging slice thickness, and 3-dimensional image plane. A separate Image Panel allows arbitrary oblique slice prescription. A "fast" real-time sequence was used for higher temporal resolution, consisting of six spiral interleaves, TR 40 msec, 240 msec per image, nominal FOV 2 cm, nominal slice thickness 5 mm, flip angle 30°, and 440 micron inplane resolution. A "slow" real-time sequence was also used for higher spatial resolution, consisting of 20 interleaves, TR 40 msec, 800 msec per image, nominal FOV 1 cm, thickness 5 mm, and 120–360 micron resolution. In addition to the real-time sequence, conventional gradient-echo and fast spin-echo imaging were performed for coil measurements, localization, and ECG-gated intravascular imaging.

Black-Blood Imaging

Real-time black-blood imaging is achieved through the use of out-of-slice saturation pulses for blood signal suppression (28) (Fig. 3). Two RF pulses (each exciting one side band) are followed by a large dephaser gradient in the slice-select direction. Typical parameters: saturation pulse flip angle-90°, saturation band thickness-4 cm, saturation deadband-1.5 cm (space between saturation band and imaging slice). The real-time control system was modified to allow interactive adjustment of slab thickness, dead band thickness, and the saturation pulse flip angle.

Catheter Coil Q and SNR Measurements

The coil quality factor (Q) was measured as the ratio of center frequency to bandwidth in both loaded (with saline) and unloaded conditions. Bandwidth was estimated as the full width at half maximum of the resistance-tuned peak (for coils tuned with a series capacitor followed by a shunt capacitor) or the capacitance-tuned peak (for coils tuned with a shunt capacitor followed by a series capacitor). Axial and coronal catheter coil sensitivity profiles were also obtained by sequentially placing each coil in the center of a 32-mm-diameter container of saline and imaging with a gradient-echo sequence: FOV 8 cm, matrix 256 × 256, TE/TR 3.8/100 msec, flip angle 60°, thickness

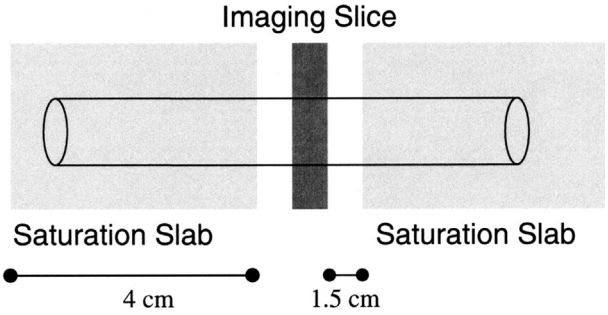

Figure 3. Real-time black-blood technique. Thick saturation slabs (typically 4 cm) are located on both sides of the imaging slice, separated by a deadband (typically 1.5 cm).

3 mm, NEX = 1. SNR gain for each catheter coil was then measured relative to a 5-inch surface coil separated from the catheter coil by 15 cm, using a 20-cm FOV. The catheter coil was placed inside a 1.25 cm tube of saline and 4-liter container of saline was placed between the catheter coil and the surface coil. A 6-mm ROI was drawn adjacent to the catheter coil to measure signal intensity.

Flow Phantom Studies

Continuous flow phantom studies were performed with the real-time intravascular imaging sequence. The catheter coils were inserted into the phantom via a 6 French introducer. The phantom consisted of an 8-mm inner diameter plastic tube surrounded by a 3-mm thick water-based silicone gel (Dow Corning Corp., Midland, MI). Water was doped with manganese chloride to simulate blood in its relaxation properties, and a constant-rate flow pump was used (Masterflex model 7520-25; Cole-Palmer Instrument Company, Chicago, IL) at a rate of 1.5 m/sec. Reference velocities were confirmed using a phase contrast sequence as previously described (28).

Ex Vivo Imaging

Ex vivo human aortae were imaged to evaluate the radial SNR and sensitivity fall-off relative to the vascular features of interest. Aortic samples were harvested at autopsy, stored in moist gauze at 4°C, and imaged within 48 hr at room temperature. A T2-weighted fast spin-echo sequence was used: FOV 4 cm, thickness 3 mm, matrix 256×256, TE eff/TR = 54/2500 msec, 16 averages, time 21:35.

In Vivo Imaging

Three male New Zealand white rabbits (3–4 kg), which have an aortic diameter (~3 mm) similar to that of human coronary arteries, were imaged under an approved protocol of the Stanford University School of Medicine Administrative Panel on Laboratory Animal Care. Animals were anesthetized with IM Ketamine (35 mg/kg), Glycopyrolate (0.02 mg/kg), and Metatomidine (250 μg/kg) to minimize pain, distress, and motion. Prior to imaging, a right iliac artery cut-down was performed and a 6F introducer was inserted. The catheter coil was then advanced into the aorta through the introducer under x-ray fluoroscopy guidance. As described above, both conventional and real-time in vivo imaging of the rabbit aorta was performed. The ECG-gated fast spin-echo sequence parameters were: FOV 4 cm, thickness 3 mm, matrix 256×256, TE 17 msec, echo-train length eight, four averages, time 1:49. At the conclusion of the MRI studies, the animals were euthanized with Beuthanasia-D solution, 0.5 mL/kg IV.

RESULTS

Catheter Coil Measurements

Table 1 shows the measured Q values of our catheter coils. The measured Q values of our first prototype coils are within the range that has been previously reported (16). The Q values for our new coax-stub matched coils are within the range one would expect for the smaller magnetic field energy per volume. The loopless probe behaved like a broadband 50 Ω resistor ($Q < 1$) and required a DC blocking capacitor to prevent electrolysis. Also shown in Table 1 are the SNR gains of these coils in saline compared to a 5-inch surface coil using identical pulse sequences. Note the favorable SNR gain of our new coil designs despite their smaller size. The loopless probe has lower near-field SNR compared to other catheter coils, as previously reported (19), despite its favorable profile.

Catheter Coil Sensitivities

Figure 4 shows the axial and longitudinal sensitivities of the coils in saline. The twin-lead coil provided the most longitudinal homogeneity (Figure 4d) with a loss in axial homogeneity and peak SNR compared to the opposed solenoids (Fig. 4b vs. 4a). The loopless coil provided the least SNR (Fig. 4c and f). The sensitivity patterns of the locally-tuned coax-stub catheter coils (Fig. 4g and h) appeared similar to those that utilize discrete capacitors.

Table 1

Catheter Coils: Measured Q, SNR Gain

Coil Configuration	Unloaded Q	Loaded Q[a]	SNR Gain
Opposed solenoid	110	60	48
Flexible twin lead	50	50	59
Loopless probe	<1	<1	4
Single solenoid[b]	47	44	34
Flexible twin lead[b]	47	41	30

[a] NaCl 150-mmol/L.
[b] Coax-Stub Matched Coils.

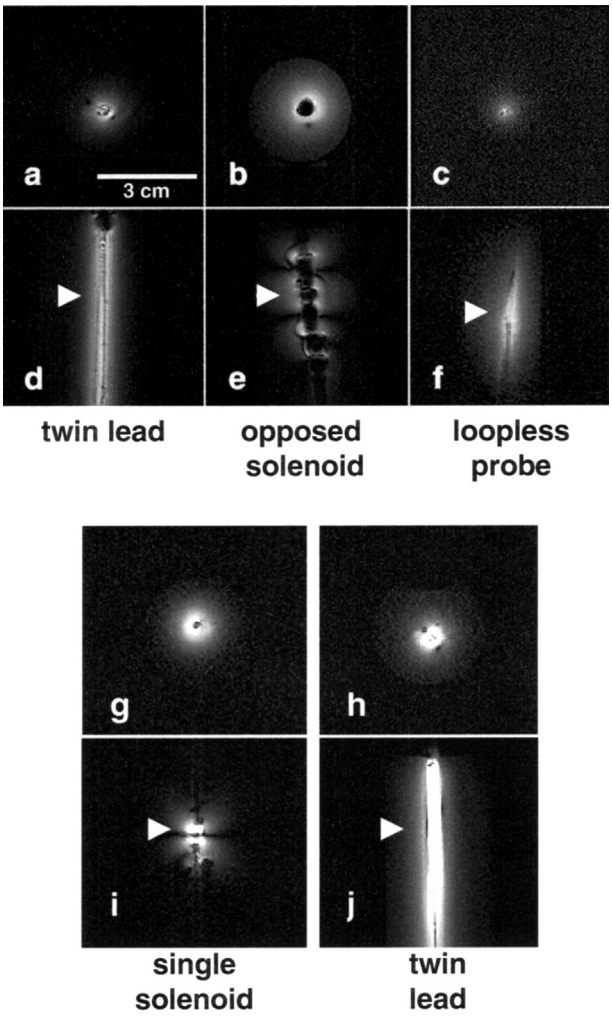

Figure 4. Coil sensitivity profiles. Axial and coronal images obtained in saline, with arrowheads on the coronal images indicating the position of the axial images. Coils in (g)–(j) utilize coaxial stub matching strategies. Note the increased longitudinal sensitivity of the twin-lead and loopless probes (d, f, j). In contrast, the solenoid designs have more uniform axial sensitivity (b, g), with limited longitudinal sensitivity (e, i).

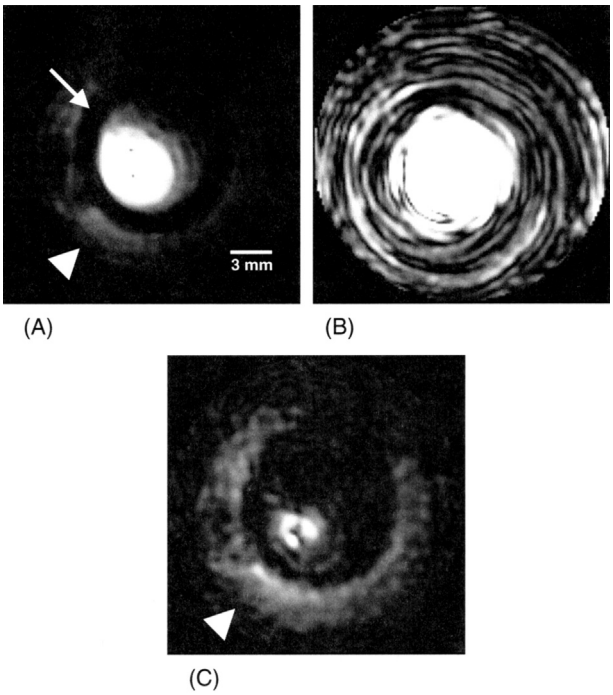

Figure 5. Real-time flow phantom experiment. (A) Flow off: Bright signal around coil, with a dark band representing the plastic wall (arrow), surrounded by a thicker gray band representing the silicone gel (arrowhead). (B) Flow on: Flow signal artifacts dominate the image. (C) Flow on, saturation pulses on: Flow signal effectively suppressed, with reduced signal around the coil. The silicone gel layer is now well seen (arrowhead), as in (A).

Flow Phantom Experiment

Real-time black-blood imaging was initially demonstrated with the coil placed in the flow phantom (Fig. 5). The phantom wall is clearly seen with flow off (Fig. 5a). When flow is turned on (without the black-blood feature), the image becomes dominated by flow-related artifacts (Fig. 5b). With the black-blood saturation pulses are turned on, flow artifacts are suppressed and the edge of the outer, water-based silicone rubber layer is visible (Fig. 5c).

Ex Vivo Imaging

An ex vivo human aorta was imaged with the twin-lead coil. (Fig. 6a) With T2-weighting, three aortic wall layers are clearly visualized, as previously described (30,31).

In Vivo Imaging

Imaging of the coil in the rabbit aorta, using conventional sequences, is shown in Fig. 6. The ECG-gated FSE image (Fig. 6c) clearly has significant artifacts related to catheter motion. Real-time in vivo intravascular images are shown in Fig. 7. The black-blood saturation pulses effectively suppress the blood flow signal, and the rabbit aortic wall is seen without motion

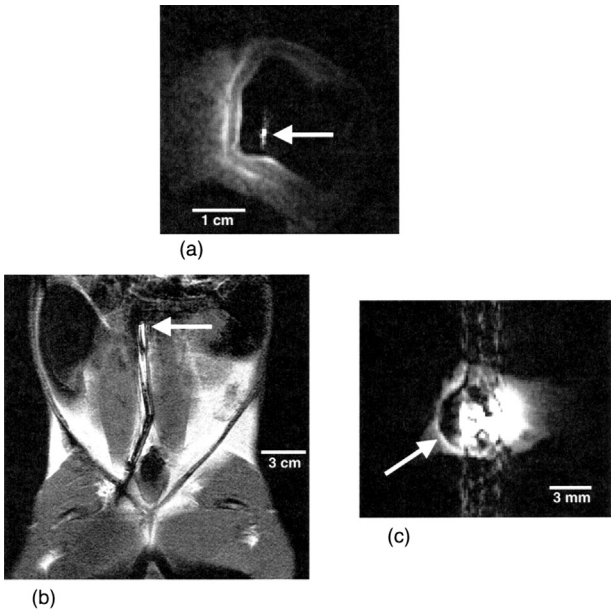

Figure 6. Nonreal-time imaging. (a) T2-weighted intravascular imaging of ex vivo human aorta at 156-μm resolution. Note the bright signal of the intravascular coil (arrow) and the adjacent three-layered vessel wall. (b) Coronal gradient-echo image, using the body coil, of a rabbit prior to intravascular imaging, showing the position of catheter coil (arrow) in the aorta via the right iliac artery. (c) Intravascular imaging of the rabbit aorta using a gated fast-spin-echo sequence at 156-μm resolution. The periadventitial fat (arrow) surrounds the thin normal aortic wall. Note the significant artifacts due to catheter motion, despite cardiac gating.

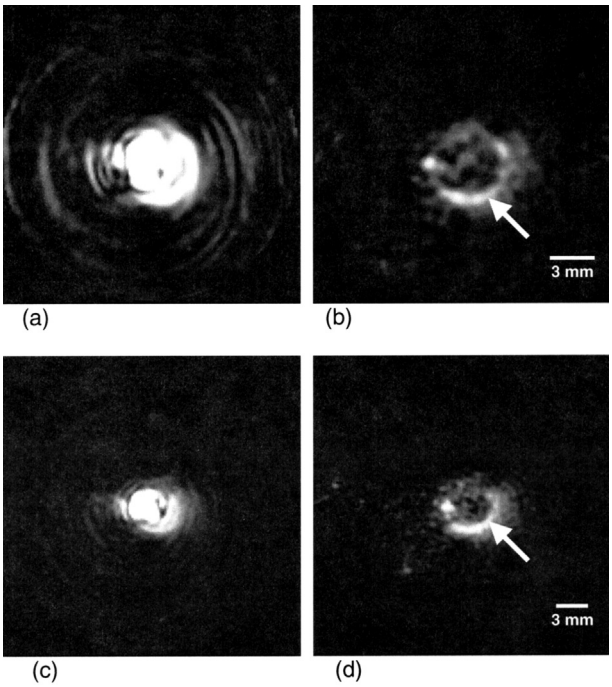

Figure 7. In vivo real-time intravascular MRI. (a) Real-time imaging in the rabbit aorta using the "fast" pulse sequence (240 msec per complete image, 440-μm resolution, 2 cm FOV) *without* saturation pulses. The blood flow signal dominates the image. (b) Intravascular imaging as in (a), except now *with* saturation pulses. Note the suppression of the blood flow signal, revealing the aortic wall (arrow). (c, d): Real-time intravascular imaging as in (a, b), except using the "slow" pulse sequence (800 msec per complete image, 360-μm resolution, 3 cm FOV). With saturation pulses on (d), the aortic wall is visualized (arrow) with good blood flow suppression. The decreased temporal resolution did not cause significant motion artifacts and allowed improved image quality at higher spatial resolution.

artifacts (Fig. 7b and d). Both "fast" and "slow" real-time sequences visualize the aortic wall, with the expected trade-offs between spatial and temporal resolution.

DISCUSSION

This is the first description of real-time, interactive intravascular MR imaging. Results demonstrate that real-time spiral acquisition and blood signal suppression methods can overcome flow- and motion-related artifacts in combination with low-profile, coaxial-stub-matched catheter coils.

The MRI of atherosclerotic plaque has made significant advances over the last decade, from ex vivo plaque characterization (30,32–36) to in vivo imaging of human carotid and aortic plaque (37–40). Coronary plaque imaging has been the most challenging, due to the small size and cardiac and respiratory motion. Recently, techniques have been developed to image the coronary wall noninvasively (10–13,41). However, the 0.5–0.8 mm spatial resolution is suboptimal for detailed assessment of coronary plaque features. In particular, fibrous cap thickness, which is correlated with risk of plaque rupture, can be on the order of 100 μ or less (42). Thus, a significant increase in sensitivity is needed to provide adequate SNR at very high spatial resolutions, leading to the development of intravascular coils.

Martin and Henkelman were the first to successfully perform intravascular MRI in vivo (21). However, to suppress motion artifacts, a 9-mm bullet-tip modification was required to limit coil motion, greatly limiting its clinical utility. A second approach involved placing an

expandable coil in an adjacent vein, the loss in SNR from radial fall-off being compensated by the potentially larger coil size (22). However, these images also suffer from motion artifacts. To overcome the size limitations of both the presence of a loop and the need for local tuning, a loopless catheter antenna with remote tuning was proposed (19). Despite its favorable low profile, the catheter's low SNR would make it impractical for real-time imaging. Another approach, involving the mounting of an intravascular coil on an inflatable balloon, was shown to provide high-resolution in vivo images of atherosclerosis (20,24). While balloon occlusion of over 3 min may be tolerated in the periphery, this would be problematic in the coronary and carotid arteries. This led to an autoperfused balloon catheter modification, which has been used to image the pig carotid artery in vivo (23). However, the use of small-diameter coaxial cables in these coil designs leads to reduced SNR. Moreover, balloon expansion exposes the vessel wall to injury and restenosis. The advantage of real-time intravascular imaging is that it allows nonocclusive, nontraumatic imaging of the vessel wall without motion artifacts.

While this study demonstrates the feasibility of real-time intravascular imaging, further improvements are required for clinical application. The quality of the in vivo images is limited, which is partially due to the very thin normal rabbit aortic wall ($<200\,\mu$). An atherosclerotic aortic wall in the rabbit can be $>500\,\mu$ (43) and would be more easily visualized. Further gains in SNR are required to allow higher spatial resolution while maintaining adequate temporal resolution. Tissue contrast methods, such as T2-weighting, need to be incorporated to allow detailed plaque characterization (30). As this study used normal rabbits, real-time in vivo plaque characterization could not be assessed. Real-time catheter tracking should also be incorporated to guide catheter placement and have the imaging plane follow as the coil is passed through the vessel of interest (44–47). Finally, catheter coils designed for human use would need to be tested for heating effects and safety.

In conclusion, real-time, interactive intravascular MRI is a promising approach to detailed, motion-free imaging of atherosclerosis in vivo. Real-time MRI is an ideal platform for catheter-based diagnosis and interventions in cardiovascular disease.

ACKNOWLEDGMENTS

Supported by grants from the National Institutes of Health (HL61864, HL39297, CA50948), the American Heart Association, the Whitaker Foundation, and the Fannie and John Hertz Foundation.

REFERENCES

1. Alderman, E.L.; Corley, S.D.; Fisher, L.D.; Chaitman, B.R.; Faxon, D.P.; Foster, E.D.; Killip, T.; Sosa, J.A.; Bourassa, M.G. Five-Year Angiographic Follow-Up of Factors Associated with Progression of Coronary Artery Disease in the Coronary Artery Surgery Study (CASS). CASS Participating Investigators and Staff. J. Am. Coll. Cardiol. **1993**, *22*, 1141–1154.
2. Ambrose, J.A.; Tannenbaum, M.A.; Alexopoulos, D.; Hjemdahl-Monsen, C.E.; Leavy, J.; Weiss, M.; Borrico, S.; Gorlin, R.; Fuster, V. Angiographic Progression of Coronary Artery Disease and the Development of Myocardial Infarction. J. Am. Coll. Cardiol. **1988**, *12*, 56–62.
3. Little, W.C.; Constantinescu, M.; Applegate, R.J.; Kutcher, M.A.; Burrows, M.T.; Kahl, F.R.; Santamore, W.P. Can Coronary Angiography Predict the Site of a Subsequent Myocardial Infarction in Patients with Mild-to-Moderate Coronary Artery Disease? Circulation **1988**, *78*, 1157–1166.
4. Mann, J.M.; Davies, M.J. Vulnerable Plaque Relation of Characteristics to Degree of Stenosis in Human Coronary Arteries. Circulation **1996**, *94*, 928–931.
5. Fuster, V.; Fayad, Z.A.; Badimon, J.J. Acute Coronary Syndromes: Biology. Lancet **1999**, *353* (Suppl. 2), SII5–SII9.
6. Libby, P. Current Concepts of the Pathogenesis of the Acute Coronary Syndromes. Circulation **2001**, *104*, 365–372.
7. Yock, P.G.; Fitzgerald, P.J. Intravascular Ultrasound: State of the Art and Future Directions. Am. J. Cardiol. **1998**, *81*, 27E–32E.
8. Martin, A.J.; Ryan, L.K.; Gotlieb, A.I.; Henkelman, R.M.; Foster, F.S. Arterial Imaging: Comparison of High-Resolution US and MR Imaging with Histologic Correlation. Radiographics **1997**, *17*, 189–202.
9. Raynaud, J.S.; Bridal, S.L.; Toussaint, J.F.; Fornes, P.; Lebon, V.; Berger, G.; Leroy-Willig, A. Characterization of Atherosclerotic Plaque Components by High Resolution Quantitative MR and US Imaging. J. Magn. Reson. Imaging **1998**, *8*, 622–629.
10. Meyer, C.H.; Hu, B.S.; Macovski, A.; Nishimura, D.G. Coronary vessel wall imaging. In: *Sixth Meeting of the International Society of Magnetic Resonance in Medicine*, Sydney, 1998; 15.
11. Fayad, Z.A.; Fuster, V.; Fallon, J.T.; Jayasundera, T.; Worthley, S.G.; Helft, G.; Aguinaldo, J.G.; Badimon, J.J.; Sharma, S.K. Noninvasive In Vivo Human Coronary Artery Lumen and Wall Imaging Using Black-Blood

Magnetic Resonance Imaging. Circulation **2000**, *102*, 506–510.
12. Botnar, R.M.; Stuber, M.; Kissinger, K.V.; Kim, W.Y.; Spuentrup, E.; Manning, W.J. Noninvasive Coronary Vessel Wall and Plaque Imaging with Magnetic Resonance Imaging. Circulation **2000**, *102*, 2582–2587.
13. McConnell, M.V.; Meyer, C.H.; Putz, E.J.; Nishimura, D.G.; Hu, B.S. Spiral Coronary Wall Imaging: Patient Studies. In: *Ninth Meeting of the International Society of Magnetic Resonance in Medicine*, Glasgow, 2001; 1969.
14. Kantor, H.L.; Briggs, R.W.; Balaban, R.S. In Vivo 31P Nuclear Magnetic Resonance Measurements in Canine Heart Using a Catheter-Coil. Circ. Res. **1984**, *55*, 261–266.
15. Hurst, G.C.; Hua, J.; Duerk, J.L.; Cohen, A.M. Intravascular (Catheter) NMR Receiver Probe: Preliminary Design Analysis and Application to Canine Iliofemoral Imaging. Magn. Reson. Med. **1992**, *24*, 343–357.
16. Martin, A.J.; Plewes, D.B.; Henkelman, R.M. MR Imaging of Blood Vessels with an Intravascular Coil. J. Magn. Reson. Imaging **1992**, *2*, 421–429.
17. Kandarpa, K.; Jakab, P.; Patz, S.; Schoen, F.J.; Jolesz, F.A. Prototype Miniature Endoluminal MR Imaging Catheter. J. Vasc. Interv. Radiol. **1993**, *4*, 419–427.
18. Atalar, E.; Bottomley, P.A.; Ocali, O.; Correia, L.C.; Kelemen, M.D.; Lima, J.A.; Zerhouni, E.A. High Resolution Intravascular MRI and MRS by Using a Catheter Receiver Coil. Magn. Reson. Med. **1996**, *36*, 596–605.
19. Ocali, O.; Atalar, E. Intravascular Magnetic Resonance Imaging Using a Loopless Catheter Antenna. Magn. Reson. Med. **1997**, *37*, 112–118.
20. Quick, H.H.; Ladd, M.E.; Zimmermann-Paul, G.G.; Erhart, P.; Hofmann, E.; von Schulthess, G.K.; Debatin, J.F. Single-Loop Coil Concepts for Intravascular Magnetic Resonance Imaging. Magn. Reson. Med. **1999**, *41*, 751–758.
21. Martin, A.J.; Henkelman, R.M. Intravascular MR Imaging in a Porcine Animal Model. Magn. Reson. Med. **1994**, *32*, 224–229.
22. Martin, A.J.; McLoughlin, R.F.; Chu, K.C.; Barberi, E.A.; Rutt, B.K. An Expandable Intravenous RF Coil for Arterial Wall Imaging. J. Magn. Reson. Imaging **1998**, *8*, 226–234.
23. Quick, H.H.; Ladd, M.E.; Hilfiker, P.R.; Paul, G.G.; Ha, S.W.; Debatin, J.F. Autoperfused Balloon Catheter for Intravascular MR Imaging. J. Magn. Reson. Imaging **1999**, *9*, 428–434.
24. Zimmermann-Paul, G.G.; Quick, H.H.; Vogt, P.; von Schulthess, G.K.; Kling, D.; Debatin, J.F. High-Resolution Intravascular Magnetic Resonance Imaging: Monitoring of Plaque Formation in Heritable Hyperlipidemic Rabbits. Circulation **1999**, *99*, 1054–1061.
25. Kerr, A.B.; Pauly, J.M.; Hu, B.S.; Li, K.C.; Hardy, C.J.; Meyer, C.H.; Macovski, A.; Nishimura, D.G. Real-Time Interactive MRI on a Conventional Scanner. Magn. Reson. Med. **1997**, *38*, 355–367.
26. Scott, G.C.; Rivas, P.A.; Hu, B. Coaxial Stub Matching Strategies for Intravascular Coils. In: *Seventh Meeting of the International Society for Magnetic Resonance in Medicine*, Philadelphia, 1999.
27. Riederer, S.J.; Tasciyan, T.; Farzaneh, F.; Lee, J.N.; Wright, R.C.; Herfkens, R.J. MR Fluoroscopy: Technical Feasibility. Magn. Reson. Med. **1988**, *8*, 1–15.
28. Nayak, K.S.; Rivas, P.A.; Pauly, J.M.; Scott, G.C.; Kerr, A.B.; Hu, B.S.; Nishimura, D.G. Real-Time Black Blood MRI Using Spatial Presaturation. J. Magn. Reson. Imaging **2001**, *13*, 807–812.
29. Nayak, K.S.; Pauly, J.M.; Kerr, A.B.; Hu, B.S.; Nishimura, D.G. Real-Time Color Flow MRI. Magn. Reson. Med. **2000**, *43*, 251–258.
30. Toussaint, J.F.; Southern, J.F.; Fuster, V.; Kantor, H.L. T2-Weighted Contrast for NMR Characterization of Human Atherosclerosis. Arterioscler. Thromb. Vasc. Biol. **1995**, *15*, 1533–1542.
31. Kaufman, L.; Crooks, L.E.; Sheldon, P.E.; Rowan, W.; Miller, T. Evaluation of NMR Imaging for Detection and Quantification of Obstructions in Vessels. Invest. Radiol. **1982**, *17*, 554–560.
32. Pearlman, J.D.; Southern, J.F.; Ackerman, J.L. Nuclear Magnetic Resonance Microscopy of Atheroma in Human Coronary Arteries. Angiology **1991**, *42*, 726–733.
33. Gold, G.E.; Pauly, J.M.; Glover, G.H.; Moretto, J.C.; Macovski, A.; Herfkens, R.J. Characterization of Atherosclerosis with a 1.5-T Imaging System. J. Magn. Reson. Imaging **1993**, *3*, 399–407.
34. Toussaint, J.F.; Southern, J.F.; Fuster, V.; Kantor, H.L. ^{13}C-NMR Spectroscopy of Human Atherosclerotic Lesions. Relation Between Fatty Acid Saturation, Cholesteryl Ester Content, and Luminal Obstruction. Arterioscler. Thromb. **1994**, *14*, 1951–1957.
35. Correia, L.C.; Atalar, E.; Kelemen, M.D.; Ocali, O.; Hutchins, G.M.; Fleg, J.L.; Gerstenblith, G.; Zerhouni, E.A.; Lima, J.A. Intravascular Magnetic Resonance Imaging of Aortic Atherosclerotic Plaque Composition. Arterioscler. Thromb. Vasc. Biol. **1997**, *17*, 3626–3632.
36. Rogers, W.J.; Prichard, J.W.; Hu, Y.L.; Olson, P.R.; Benckart, D.H.; Kramer, C.M.; Vido, D.A.; Reichek, N. Characterization of Signal Properties in Atherosclerotic Plaque Components by Intravascular MRI. Arterioscler. Thromb. Vasc. Biol. **2000**, *20*, 1824–1830.
37. Toussaint, J.F.; LaMuraglia, G.M.; Southern, J.F.; Fuster, V.; Kantor, H.L. Magnetic Resonance Images Lipid, Fibrous, Calcified, Hemorrhagic, and Thrombotic Components of Human Atherosclerosis In Vivo. Circulation **1996**, *94*, 932–938.
38. Fayad, Z.A.; Nahar, T.; Fallon, J.T.; Goldman, M.; Aguinaldo, J.G.; Badimon, J.J.; Shinnar, M.; Chesebro,

J.H.; Fuster, V. In Vivo Magnetic Resonance Evaluation of Atherosclerotic Plaques in the Human Thoracic Aorta: A Comparison with Transesophageal Echocardiography. Circulation **2000**, *101*, 2503–2509.
39. Hatsukami, T.S.; Ross, R.; Polissar, N.L.; Yuan, C. Visualization of Fibrous Cap Thickness and Rupture in Human Atherosclerotic Carotid Plaque In Vivo with High-Resolution Magnetic Resonance Imaging. Circulation **2000**, *102*, 959–964.
40. Fattori, R.; Nienaber, C.A. MRI of Acute and Chronic Aortic Pathology: Pre-Operative and Postoperative Evaluation. J. Magn. Reson. Imaging **1999**, *10*, 741–750.
41. Worthley, S.G.; Helft, G.; Fuster, V.; Fayad, Z.A.; Rodriguez, O.J.; Zaman, A.G.; Fallon, J.T.; Badimon, J.J. Noninvasive In Vivo Magnetic Resonance Imaging of Experimental Coronary Artery Lesions in a Porcine Model. Circulation **2000**, *101*, 2956–2961.
42. Virmani, R.; Kolodgie, F.D.; Burke, A.P.; Farb, A.; Schwartz, S.M. Lessons from Sudden Coronary Death: A Comprehensive Morphological Classification Scheme for Atherosclerotic Lesions. Arterioscler. Thromb. Vasc. Biol. **2000**, *20*, 1262–1275.

Received October 10, 2000
Accepted August 20, 2001

43. McConnell, M.V.; Aikawa, M.; Maier, S.E.; Ganz, P.; Libby, P.; Lee, R.T. MRI of Rabbit Atherosclerosis in Response to Dietary Cholesterol Lowering. Arterioscler. Thromb. Vasc. Biol. **1999**, *19* (8), 1956–1959.
44. Dumoulin, C.L.; Souza, S.P.; Darrow, R.D. Real-Time Position Monitoring of Invasive Devices Using Magnetic Resonance. Magn. Reson. Med. **1993**, *29*, 411–415.
45. Ladd, M.E.; Zimmermann, G.G.; Quick, H.H.; Debatin, J.F.; Boesiger, P.; von Schulthess, G.K.; McKinnon, G.C. Active MR Visualization of a Vascular Guidewire In Vivo. J. Magn. Reson. Imaging **1998**, *8*, 220–225.
46. Atalar, E.; Kraitchman, D.L.; Carkhuff, B.; Lesho, J.; Ocali, O.; Solaiyappan, M.; Guttman, M.A.; Charles, H.K., Jr. Catheter-Tracking FOV MR Fluoroscopy. Magn. Reson. Med. **1998**, *40*, 865–872.
47. Nayak, K.S.; Rivas, P.R.; McConnell, M.V.; Santos, J.M.; Scott, G.C.; Nishimura, D.G.; Pauly, J.M.; Hu, B.S. Real-Time Black-Blood Imaging and Active Tracking for Catheter-Based MRI. In: *Fourth Meeting of the Society for Cardiovascular Magnetic Resonance*, Atlanta, 2001; 134.